BULLETIN OF THE POLISH ACADEMY OF SCIENCES
TECHNICAL SCIENCES, Vol. 71(6), 2023, Article number: e147344
DOI: 10.24425/bpasts.2023.147344

Research on improved sparrow search algorithm for PID controller parameter optimization

Mingfeng ZHANG[1], Chuntian XU[1]*, Deying XU[1], Guoqiang MA[1], Han HAN[2], and Xu ZONG[3]

[1] School of Mechanical Engineering and Automation, University of Science and Technology Liaoning, Anshan, Liaoning, China
[2] College of Science – Computer Science, University of Arizona, Tucson, Arizona, USA
[3] Angang Steel Co. LTD, Anshan Iron & Steel, Anshan, Liaoning, China

Abstract. PID controllers are crucial for industrial control because of their simple structure and good robustness. In order to further improve the accuracy of PID controllers, this paper proposes an improved sparrow search algorithm (ISSA) to prevent the problem of the algorithm being prone to falling into the local optimum at the late stage of iteration. Based on the standard sparrow search algorithm, the position update formula and the step size control parameter are optimized to help quickly jump out of the local, and to obtain the optimal solution in the whole domain. Finally, to verify the accuracy and stability of the improved algorithm, nine standard test functions are first simulated. Then, the PID parameter optimization tests are finished with the chilled water and battery charging systems, where the lifting load and applying perturbation are carried out. Both the simulation and test results show that ISSA improves the convergence speed and accuracy, and performs better in terms of stability.

Key words: improved sparrow search algorithm; PID controller; parameter optimization.

1. INTRODUCTION

In recent years, with the rapid development of artificial intelligence, group intelligence algorithms have also received more and more attention from scholars [1]. These algorithms, with fewer parameters, relatively simple evolutionary processes, fast computing speed and strong global search capability, have been widely used in research and engineering. The simplicity, transparency, reliability, efficiency and robustness of PID controllers is one of the reasons for their high popularity and acceptance in the process industries around the world today.

The advantages of PID controllers are welcomed and accepted in industrial process control [2]. However, the conventional PID parameter optimization method has not been able to fully adapt to the requirements of the development of intelligent control, thus many researchers, through the introduction of group intelligence algorithms, optimize the parameters of PID to improve its control performance. Literature [3] used a genetic algorithm to optimize the parameters of nonlinear PID for a 6-degree-of-freedom UAV quadrotor system. Literature [4] also optimized the parameters of PID for a continuously stirred reactor by the modified hybrid artificial bee colony algorithm with good results. In another study, literature [5] used the moth flame optimization algorithm for variable range optimization of PID controller parameters for fractional range control schemes to regulate the temperature of the mixing process. The controller parameters were optimized using the Ziegler–Nichols method and the moth flame optimization algorithm for different temperature setpoints, and it was found that the moth flame optimization algorithm optimization method provided significant improvements by analyzing the performance at a single temperature setpoint. For optimizing the best parameters of PID speed and current for switched reluctance motors, literature [6] presented a smart bacterial foraging optimization algorithm. The results show that when the parameters of the PID controller are optimized using this algorithm, the maximum dynamic response increased average torque and minimized current pulsations are obtained. In order to improve the response characteristics of the magnetorheological fluid brake and to reduce the braking fluctuation rate, an enhanced grey wolf optimization algorithm named EGWOA is proposed in the literature [7] for tuning the parameters of the PID controller. It is shown through simulations and experiments that the EGWOA has a faster response output and better overall performance. Based on an improved particle swarm algorithm, literature [8] demonstrated that the parameter optimization of fractional order PID controller has a faster search speed and better solution than a genetic algorithm. In order to achieve the speed control of a permanent magnet synchronous motor, literature [9] optimized the PID control parameters of a permanent magnet synchronous motor with an ant lion optimization algorithm. In another study, literature [10] used the flower pollination algorithm for PID speed control of brushless DC motors. And the experimental comparisons revealed its superior performance characteristics as compared to traditional methods. For the traditional air suspension PID controller, existing in too long adjustment time and experiencing an obvious overshooting phenomenon in the body height adjustment process, literature [11] designed a seeker optimization algorithm based on the PID transverse in-

*e-mail: xuchuntian@163.com

Manuscript submitted 2023-04-17, revised 2023-08-31, initially accepted for publication 2023-09-22, published in December 2023.

terconnection of electronic control of the air suspension system controller. The test results show that this method effectively improves the smoothness and operational stability of the vehicle. In addition, the seagull optimization algorithm [12] and cuckoo search algorithm [13] have also been used to optimize the PID parameters with some success.

The sparrow search algorithm (SSA) [14] is a new type of an intelligent optimization algorithm and it has been successfully applied to several engineering fields. Literature [15] applied ISSA to entropy-based image segmentation and verified the effectiveness of the method with classical and medical images. Based on SSA, literature [16] proposed a bio-inspired path-planning method for mobile robots and verified that the method could plan more straightforward routes. For the UAV route planning problem, literature [17] proposed a modified sparrow search algorithm called CASSA for solving the problem. The results show that CASSA can solve the UAV path planning problem more efficiently in the same environment. In another study, literature [18] proposed a hybrid improved SSA for dissolved oxygen prediction and control in aquaculture by modifying the position update strategy and introducing the Cauchy mutation strategy and greedy rule in SSA (HISSA). The simulation results show that the proposed HISSA has strong effectiveness and practicality for engineering parameter optimization. Combining tent chaotic mapping, quantum behavioral strategy and Gaussian variation, literature [19] proposed a chaotic quantum sparrow search algorithm, in which the proposed high accuracy and good adaptability of the algorithm were verified and the parameters of the FOM battery model were identified. Literature [20] fused Kent chaotic mapping, t-distribution and Lévy flight strategy to obtain an improved chaotic sparrow search algorithm (ICSSA). It is used to identify the parameters of the robotic arm with an unknown load and shows that ICSSA provides more competitive results as compared to other classical algorithms.

However, SSA produces a large number of invalid sparrows in engineering applications [21] as well as a tendency to fall into local optimality when searching close to the global optimum, and a decrease in population diversity in the later stages of the algorithm [22]. These have not been well solved so far, thus affecting PID controller accuracy. To this end, this paper proposes an improved sparrow search algorithm (ISSA) by optimizing the position update formula and the step control parameter formula. To verify the effectiveness of ISSA, it is tested with nine standard functions and PID controller parameters, respectively. The results show that the optimization performance of ISSA is better, and there is a significant improvement in optimizing PID parameters.

2. IMPROVED SPARROW SEARCH ALGORITHM

2.1. Standard sparrow search algorithm

SSA is a novel algorithm obtained by simulating the foraging behavior of sparrows in nature. According to its role in the population, a sparrow can be categorized into a discoverer, scrounger or a vigilante, and each position of the sparrow corresponds to a solution. The optimal solution of the algorithm is found by constantly updating the position and fitness function of the discoverer, scrounger and vigilante, respectively. Their positions corresponding to the updating formulas are respectively expressed as:

$$X_{i,j}^{i+1} = \begin{cases} X_{i,j}^{t} \cdot \exp\left(-\dfrac{i}{\alpha \cdot \mathrm{iter}_m}\right) & (R_2 < ST), \\ X_{i,j}^{t} + Q \cdot L & (R_2 \geq ST), \end{cases} \tag{1}$$

$$X_{i,j}^{i+1} = \begin{cases} Q \cdot \exp\left(\dfrac{X_w^t - X_{i,j}^t}{i^2}\right) & \left(i > \dfrac{n}{2}\right), \\ X_p^{t+1} + \left|X_{i,j}^t - X_p^{t+1}\right| \cdot A^+ \cdot L & \left(i \leq \dfrac{n}{2}\right), \end{cases} \tag{2}$$

$$X_{i,j}^{i+1} = \begin{cases} X_b^t + \beta \left|X_{i,j}^t - X_b^t\right| & (f_i < f_g), \\ X_{i,j}^t + K \cdot \left(\dfrac{\left|X_{i,j}^t - X_w^t\right|}{(f_i - f_w) + \varepsilon}\right) & (f_i = f_g), \end{cases} \tag{3}$$

where t represents the current number of iterations; $X_{i,j}$ is the position information of the i-th sparrow in the j-th dimension; $iter_m$ is the maximum number of iterations; α is a random number of $[0,1]$; Q is a random number obeying normal distribution; L is a $1 \times n$ matrix, and each element of the matrix is one and n is the number of populations; R_2 ($R_2 \in [0,1]$) and ST ($ST \in [0.5, 1]$) denote the warning and safety values, respectively; X_w is the current global worst position; X_p is the optimal position currently occupied by the discoverer; A is a $1 \times n$ matrix with each element randomly assigned to 1 or –1 and $A^+ = A^T(AA^T)^{-1}$; X_b is the current global optimal position; β is a random number that follows a normal distribution with mean 0 and variance 1; $K \in [-1,1]$ is a random number; f_i is the current sparrow fitness value; f_g and f_w are the current global best and worst fitness values, respectively; and ε is the smallest constant allowing to avoid a zero denominator.

Except for the discoverers, the rest of the sparrows are all scroungers. In the case of scroungers $i > n/2$, the i-th scrounger does not get food and needs to fly to other places to feed. Between 10% and 20% of the discoverers and scroungers are randomly selected as vigilantes.

2.2. Improved sparrow search algorithm (ISSA)

The discoverer position at the next moment in the SSA iteration process depends on where it was at the previous moment. From equation (1), it can be seen that when $R_2 < ST$, if there are no predators around the environment where the population is searching, the discoverer will have a comprehensive search range. A broad search is performed over the entire search space, and if the position of X_i at moment t is poor, the corresponding position at moment $t+1$ is also poor, which may produce invalid individuals. To do this, the discoverer position equation (1) is modified and updated as follows:

$$X_{i,j}^{i+1} = \begin{cases} \left|X_{i,j}^t - X_b^t\right| \cdot \exp\left(-\dfrac{i}{\alpha \cdot \mathrm{iter}_m}\right) & (R_2 < ST), \\ X_{i,j}^t + Q \cdot L & (R_2 \geq ST). \end{cases} \tag{4}$$

The modified discoverer position equation (4) shows that when $R_2 < ST$, the discoverer performs a random search within the range of its position and the current global optimal location, and thus, its global search capability is enhanced.

From equation (2), SSA has a direction of only 1 or –1 when the scrounger immediately follows the discoverer during the iteration process. When the scrounger competes with the discoverer for food and wins, the scrounger becomes the discoverer, which makes the later iterations of the algorithm prone to local optimization and poor population diversity. For this, a normally distributed random number Q is introduced at $i \le n/2$ to enhance the multiplicity of the search directions of the scroungers in order to improve search accuracy. The formula for updating the position of scroungers is as follows:

$$X_{i,j}^{i+1} = \begin{cases} Q \cdot \exp\left(\dfrac{X_w^t - X_{i,j}^t}{i^2}\right) & \left(i > \dfrac{n}{2}\right), \\ X_p^{t+1} + X_p^{t+1} \cdot Q & \left(i \le \dfrac{n}{2}\right). \end{cases} \tag{5}$$

Accordingly, the vigilante position update formula is:

$$X_{i,j}^{i+1} = \begin{cases} X_b^t + \beta \left| X_{i,j}^t - X_b^t \right| & (f_i < f_g), \\ X_{i,j}^t + K \cdot \left| X_{i,j}^t - X_w^t \right| & (f_i = f_g). \end{cases} \tag{6}$$

And the step control parameter K is calculated as follows:

$$K = \exp\left(-2 \cdot \tan\left(\frac{i}{\text{iter}_m}\right)\right) \cdot (2 \cdot \gamma - 1), \tag{7}$$

where γ is a random number in the range of $[0, 1]$.

K with the number of iterations change rule is shown in Fig. 1. Its positive and negative values indicate the direction of the search, and tend to zero throughout the search process, which helps to improve the convergence speed of the algorithm. The ISSA equation (4)–(7) show that if the vigilante is in the optimal position, it jumps to a random position between its current and the global worst to search for an optimum. Otherwise, it jumps to a random position between its current and global optimum to find an optimum. And thus, the probability of algorithm falling into the local optimum is reduced.

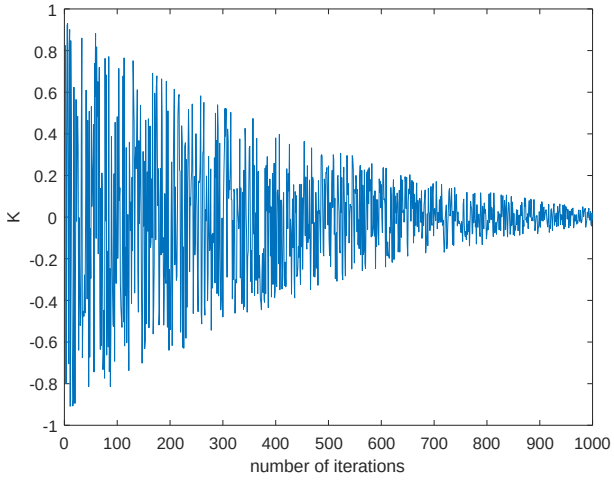

Fig. 1. Schematic of the variation of the random number K with the number of iterations

The flowchart of the improved sparrow search algorithm is shown in Fig. 2.

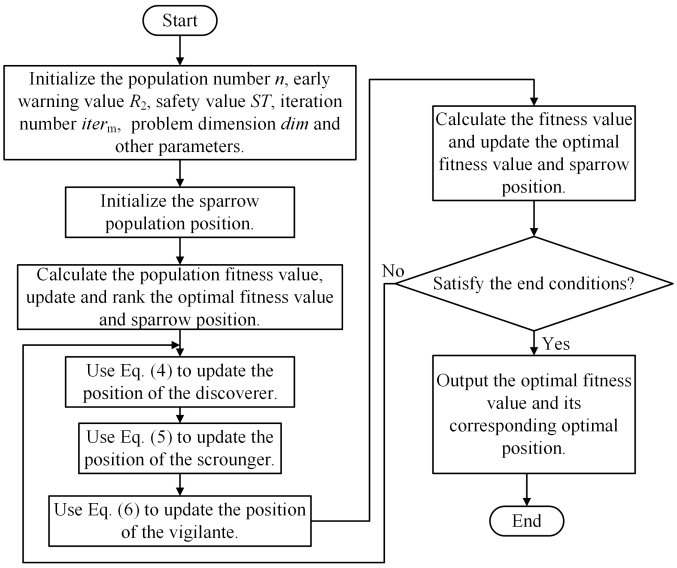

Fig. 2. ISSA algorithm optimization flowchart

3. STANDARD TEST FUNCTION VALIDATION

3.1. Test algorithm

In order to verify the feasibility and advancement of ISSA, the particle swarm optimization algorithm£šPSO£©, grey wolf optimization algorithm (GWO), whale optimization algorithm (WOA) and SSA are selected to perform a comprehensive comparison under nine standard test functions, which are shown in Table 1. After simulation verification in Matlab, the optimal setup parameters for each algorithm are obtained as follows for all of them: PSO: the learning factors $c1$ and $c2$ are 1.5 and the inertia weights $\omega = 0.9$; GWO: algorithm convergence factor $a = [2, 0]$; WOA: $a = [2, 0]$, $r1$, $r2$ both belong to $[0, 1]$; SSA and ISSA: discoverers as a proportion of population size $PD = 0.2$, vigilantes as a proportion of population size $SD = 0.2$, safety value $ST = 0.8$.

The simulation tests are performed using Windows 10 Home Chinese edition, an Intel(R) Core (TM) *i*5-8300 H processor running at 2.30 GHz, a 64-bit operating system, and 16 GB of RAM. The population size of all algorithms is set to 30, and the maximum number of iterations is 500.

3.2. Experimental results and analysis

The average and standard deviation (Std) for 30 runs of each algorithm is computed for each of the nine test functions to increase the credibility of the simulation findings. Each algorithm is independently performed 30 times on each benchmark test function. The average value reflects the convergence accuracy that each algorithm can achieve, and standard deviation reflects the stability of each algorithm. The statistical results are

Table 1
Benchmark test function

Types	Function expressions	Dimensional	Value range	Optimal solution
Uni-modal	$F_1(x)=\sum_{i=1}^{n}x_i^2$	30	$[-100,100]$	0
	$F_2(x)=\sum_{i=1}^{n}\left(\prod_{j=1}^{i}\lvert x_i\rvert\right)^2$	30	$[-100,100]$	0
	$F_3(x)=\sum_{i=1}^{n}ix_i^4+\text{random}(0,1)$	30	$[-1.28,1.28]$	0
Multi-modal	$F_4(x)=\sum_{i=1}^{n}-x_i\sin(\sqrt{\lvert x_i\rvert})$	30	$[-500,500]$	$-418.9829\times n$
	$F_5(x)=-20\exp\left(-0.2\sqrt{\frac{1}{n}\sum_{i=1}^{n}x_i^2}\right)-\exp\left(\frac{1}{n}\sum_{i=1}^{n}\cos(2\pi x_i)\right)+20+e$	30	$[-32,32]$	0
	$F_6(x)=\frac{1}{4000}\sum_{i=1}^{n}x_i^2-\prod_{i=1}^{n}\cos\left(\frac{x_i}{\sqrt{i}}\right)+1$	30	$[-600,600]$	0
Fixed-dimension multimodal	$F_7(x)=\sum_{i=1}^{11}\left[a_i-\frac{x_1(b_i^2+b_ix_2)}{b_i^2+b_ix_3+x_4}\right]$	4	$[-5,5]$	0.0003
	$F_8(x)=-\sum_{i=1}^{4}c_i\exp\left(-\sum_{j=1}^{3}a_{ij}(x_j-p_{ij})^2\right)$	3	$[1,3]$	–3.86
	$F_9(x)=-\sum_{i=1}^{7}\left[(x-a_i)(x-a_i)^T+c_i\right]^{-1}$	4	$[0,10]$	–10.5363

shown in Table 2, where bold is the optimal value. In order to compare the convergence speed of ISSA in solving benchmark test functions, the average convergence curves of the five algorithms in solving nine benchmark test functions are given in Fig. 3; the y-axis is logarithmic to render the data fluctuations precise.

From the experimental results in Table 2, it can be found that for the uni-modal test functions $F1$ to $F3$, the average values of each standardized test function solved by ISSA are the closest to the optimal solution given in Table 1, and the standard deviations are all smaller than those of the remaining four algorithms. Also, from the average convergence graph in Fig. 3, it can be seen that the convergence speed of ISSA on the $F1$, $F2$ and $F3$ benchmark test functions is also distinctly better than the remaining four algorithms. The above show that ISSA performs overall better than the remaining four algorithms regarding convergence accuracy, stability and convergence speed on the uni-modal test function. For the multi-modal test functions, it can be seen from Table 2 and the average convergence curves in Fig. 3 that ISSA is better than the remaining four al-

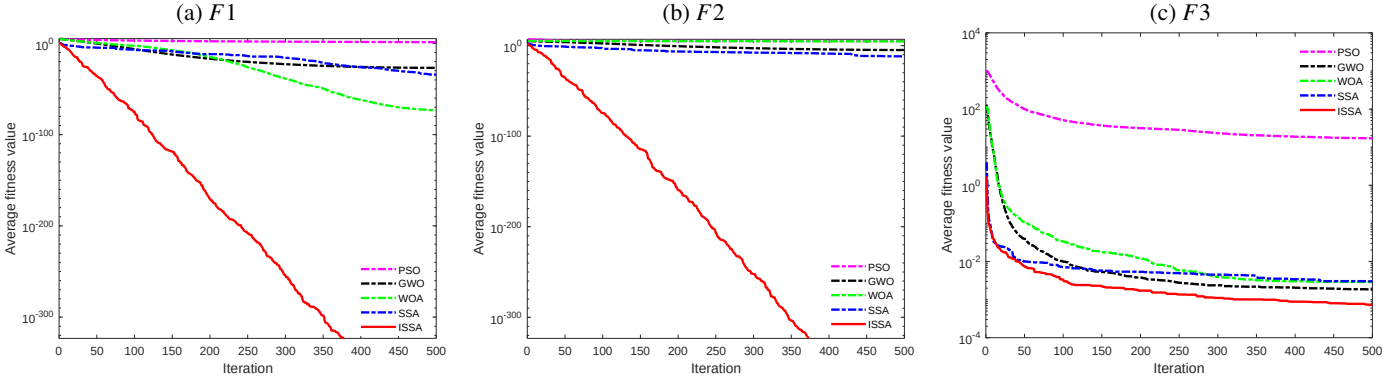

Fig. 3

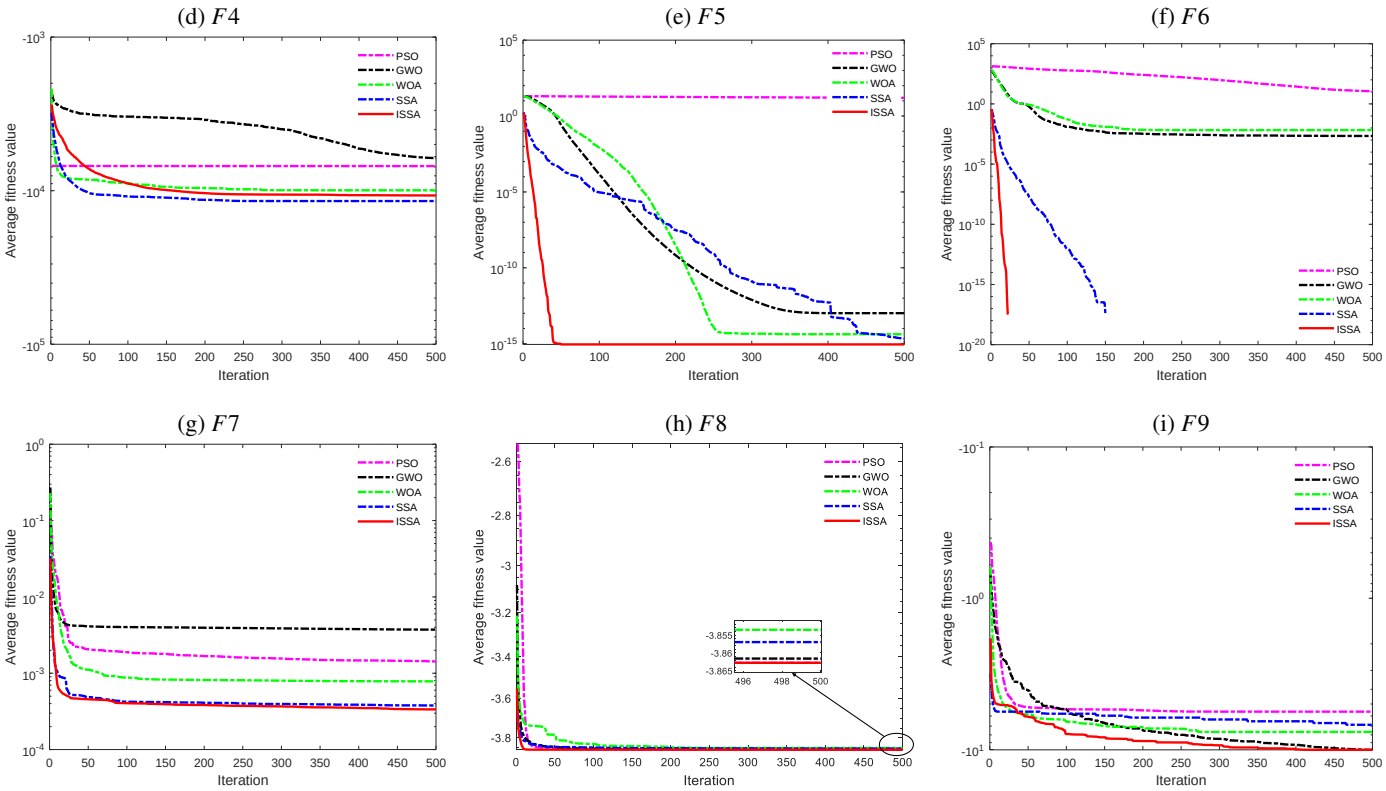

Fig. 3. Average convergence curves of five algorithms under nine test functions

Table 2
Optimization result of each algorithm in benchmark test function

Function code	Statistic	PSO	GWO	WOA	SSA	ISSA
*F*1	Average	19.9	1.54e–27	5.37e–74	5.22e–35	**0**
	Std	7.30	2.63e–27	2.09e–73	2.81e–34	**0**
*F*2	Average	9.78e4	1.18e–05	4.43e4	1.27e–12	**0**
	Std	1.28e5	2.18e–05	1.38e4	6.77e–12	**0**
*F*3	Average	17.0	1.84e–3	2.90e–3	3.02e–3	**7.24e–4**
	Std	32.2	0.939e–3	4.31e–3	3.16e–3	**0.658e–3**
*F*4	Average	–6.92e3	–5.93e3	–1.02e4	**–1.24e4**	–1.09e4
	Std	1.32e3	1.03e3	1.83e3	0.774e3	**0.603e3**
*F*5	Average	15.9	1.02e–13	4.20e–15	2.19e–15	**8.88e–16**
	Std	6.62	1.82e–14	2.23e–15	2.51e–15	**0**
*F*6	Average	11.3	2.17e–3	6.69e–3	**0**	**0**
	Std	26.9	0.574e–2	3.60e–2	**0**	**0**
*F*7	Average	1.43e–3	3.73e–3	0.784e–3	0.376e–3	**0.335e–3**
	Std	2.97e–4	7.44e–3	4.76e–4	1.49e–4	**8.00e–05**
*F*8	Average	–3.86	–3.86	–3.85	–3.86	–3.86
	Std	9.04e–06	2.41e–3	2.15e–2	9.13e–3	**2.24e–15**
*F*9	Average	–5.62	–10.1	–7.64	–6.86	**–10.1**
	Std	1.59	1.32	2.94	2.51	**1.31**

gorithms in terms of average, standard deviation, and convergence speed for solving$F5$ and $F6$; for function $F4$, although ISSA does not perform as well as SSA in terms of average and convergence speed, its standard deviation is the smallest of the five algorithms. The above show that the overall performance of ISSA in the multi-modal test function is also better. For the fixed-dimensional multimodal test function, ISSA outperforms the remaining four algorithms in terms of average, standard deviation, and convergence speed in solving functions $F7$ and $F9$; for function $F8$, all five algorithms can search for the optimal value efficiently, and the comparison of average values reveals that ISSA and PSO are the closest to the optimal solution, while the average value of WOA is the worst; the standard deviation of ISSA is improved by more than ten orders of magnitude as compared to the remaining four algorithms, which is the best in terms of stability. Also, the convergence graph in Fig. 3 shows that ISSA has the fastest convergence rate. The above show that ISSA also performs better in convergence accuracy, stability and convergence speed in fixed dimensional multi-modal test functions.

4. PID CONTROLLER PARAMETER OPTIMIZATION

PID controllers have been widely used in the industrial field for their advantages of precise structure and good robustness. Parameters setting in PID controllers will significantly affect the quality of the controllers. Thus, the optimization of PID parameters with ISSA is essentially to determine a set of suitable values of K_p, K_i and K_d, within a limited range to make the indicators of the system reach their optimums. The schematic diagram of ISSA-optimized PID parameters is shown in Fig. 4.

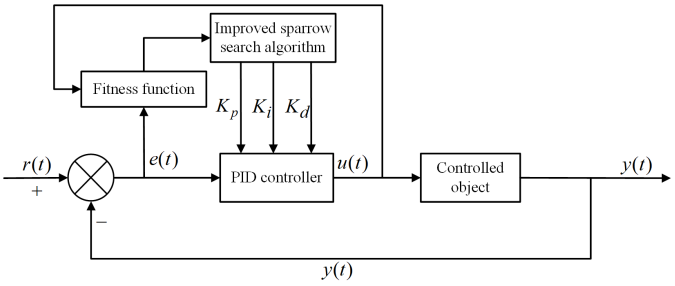

where $r(t)$ is a given value; $u(t)$ is the output of the PID controller; y(t) is an actual output value and $e(t)$ is the system deviation.

Fig. 4. ISSA optimization of PID parameters – schematic diagram

The continuous form of a PID controller is described as follows:

$$u(t) = K_p e(t) + K_i \int_0^t e(t)\,\mathrm{d}t + K_d \frac{\mathrm{d}e(t)}{\mathrm{d}t}, \tag{8}$$

where $e(t)$ means:

$$e(t) = r(t) - y(t).$$

Letting the sampling instant replace continuous time and discretizing the integral and differential terms [22], the discrete form of a PID controller is written as:

$$u(k) = K_p e(t) + K_i \sum_0^k e(k) + K_d [e(k) - e(k-1)], \tag{9}$$

where k is the sampling sequence; $u(k)$ is the controller output at the k^{th} sampling moment; $e(k)$ is the deviation value of the input at the k^{th} sampling moment; and $e(k-1)$ is the deviation of the input at the $(k-1)$ sampling moment.

Three types of gains can be seen in equation (9), that is, proportional gain (K_p), integral gain (K_i) and differential gain (K_d), and the magnitude of these three gains directly affects stability of the system.

The fitness function is used to measure the control effectiveness of a PID control system. Its selection directly affects overall performance of the system. The smaller the value of the fitness function, the more suitable the K_p, K_i and K_d found by the intelligent algorithm, and the better the overall performance of the control system. In order to obtain more satisfactory performance of the system, the absolute value of the error time-integrated performance index is utilized as the minimum objective function for parameter selection. Meanwhile, to avoid the output $u(t)$ of the PID controller becoming too large, the square term of $u(t)$ is added to the objective function, and the fitness function used is [24]:

$$J(t) = \int_0^\infty (\omega_1 |e(t)| + \omega_2 u^2(t))\,\mathrm{d}t, \tag{10}$$

Noticeably, if an overshooting is generated, a overshooting term $\omega|e(t)|$ is essentially introduced into the fitness function $J(t)$. At this point, the fitness function is shown in equation (11):

$$J(t) = \int_0^\infty (\omega_1 |e(t)| + \omega_2 u^2(t))\,\mathrm{d}t + \omega_3 |e(t)|, \tag{11}$$

where ω_1, ω_2, ω_3 are the weights, ω_1, $\omega_2 \in [0,1]$ and $\omega_1 \ll \omega_3$, and in general, $\omega_1 = 0.999$, $\omega_2 = 0.001$, $\omega_3 = 100$; $u(t)$ is the output of the PID controller.

ISSA is used to optimize the parameters of the PID controller, and the position of each sparrow can be denoted as K_p, K_i, K_d, respectively. The optimal fitness value is searched for in the population through the initialization of the population by ISSA, the calculation of fitness value, and the iterative search for the optimal number. And then, the solutions corresponding to the optimal fitness value are assigned to K_p, K_i, K_d, respectively, and the fitness function curve as well as the unit step response curve are drawn at last. The flow chart of ISSA-optimized PID controller parameters is shown in Fig. 5.

ISSA is used to optimize the PID controller parameters with equation (11) as the fitness function, and its objective is to find a set of PID values that minimizes the $J(t)$ error by correcting K_p, K_i and K_d.

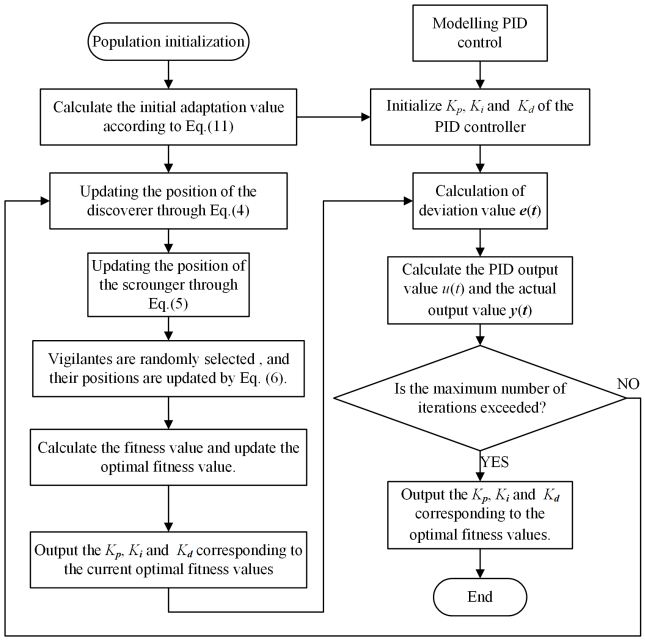

Fig. 5. Optimization of PID controller parameters by ISSA

5. EXAMPLES AND SIMULATION RESULTS

In process control, many systems are often approximated as first or second order systems. In order to further test the effect of ISSA optimization on PID parameters, the chilled water control system and battery charging system are used to establish the conventional PID controller (PID), differential evolutionary algorithm PID controller (DE-PID), particle swarm optimization algorithm PID controller (PSO-PID), ant lion optimization algorithm PID controller (ALO-PID) and the improved sparrow search algorithm PID controller (ISSA-PID) for the comparison of parameter optimization. The conventional PID controller parameters are derived from the Ziegler–Nichols (Z–N) tuning method.

In order to better measure the strengths and weaknesses of ISSA in optimizing the PID parameters, here four dynamic performance metrics of the unit step response of the closed-loop system were selected [25]: maximum overshoot σ (%), peak time t_p, rise time t_r and stable time t_s (minimum time to stabilize within $\pm 2\%$ error).

Moreover, the four intelligent algorithms have a population size of 50, a maximum number of iterations of 50, and a dimension of 3 dimensions. After simulation verification in Matlab, the optimal setup parameters for each algorithm are obtained as follows for all of them: DE: threshold $yz = 10^{-6}$, crossover operator $CR = 0.1$, and initial variation operator $F_0 = 0.4$; PSO: inertia weight $\omega = 0.9$ and learning factors $c_1 = c_2 = 1.5$; ISSA: discoverers as a proportion of population size $PD = 0.2$, vigilantes as a proportion of population size $SD = 0.2$ and safety value $ST = 0.8$.

In practical application environments, different perturbations are often encountered, and the cause of the perturbations may be caused by human control requirements or uncertain [26]. Therefore, ISSA is tested for lift loads and perturbations to verify the robustness of this algorithm.

5.1. Chilled water control system

Chilled water control system, due to the end of the cold load, is always in dynamic change, so it has a large hysteresis and multi-interference, and shows other characteristics of the conventional PID control effect rather poorly. The mathematical model can be simplified to a second order model with a time lag. The mathematical model of the chilled water system is as follows:

$$G(s) = \frac{Ke^{-\tau s}}{(T_1 s + 1)(T_2 s + 1)}, \tag{12}$$

T_1 and T_2 are inertia time coefficients; K is the amplification factor, and τ is the pure lag time parameter of the chilled water system.

For the value of the coefficients in equation (12), the chilled water system model values in the literature [27] are used, along with the transfer function of the chilled water system with numerical values in equation (13).

$$G(s) = \frac{12}{50s^2 + 51s + 1} e^{-30s}, \tag{13}$$

The Z–N tuning method is used to adjust the chilled water system PID controller parameters after several tests to get the conventional PID parameters: $K_p = 0.1105$, $K_i = 0.001$ and $K_d = 0.012$. When the four intelligent algorithms are used for system PID control, the sampling time is 5 seconds(s); the simulation time is 1000 s, and K_p, K_i, $K_d \in [0, 1]$. The unit step response curves of the five PID controllers for this chilled water control system are output and use the unit step signal as input.

Table 3 shows the PID parameters of the five controllers. Figure 6 compares the control effects. The convergence curve is shown in Fig. 7. The Bode curve is shown in Fig. 8. The performance index of each algorithm is shown in Table 4.

Table 3
PID parameters

Algorithm	K_p	K_i	K_d	$J(t)$
PID	0.1105	0.001	0.012	–
DE-PID	0.0591	0.00122	0.312	16.2699
PSO-PID	0.0591	0.00079	0.00001	21.2074
ALO-PID	0.0467	0.00096	0.4232	18.3232
ISSA-PID	0.08912	0.001537	0.7815	10.8591

Table 4
Performance index

Algorithm	σ(%)	t_p (s)	t_r (s)	t_s (s)
PID	3.356	100.5	78	466.3
DE-PID	1.8466	205	120	140
PSO-PID	0	1200	235	435
ALO-PID	0.5658	325	165	220
ISSA-PID	0.0107	230	85	110

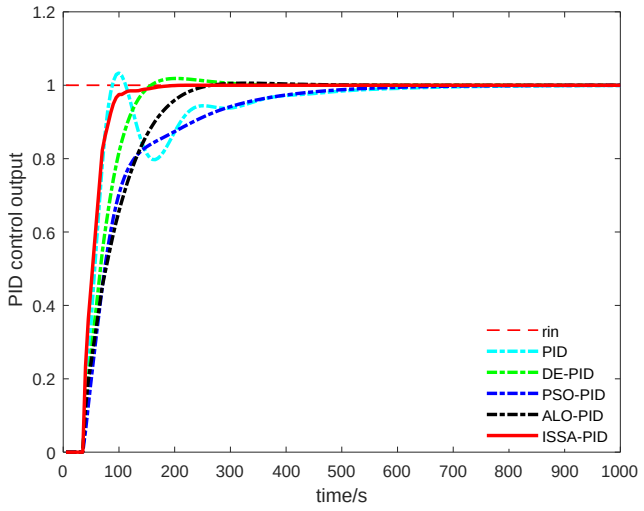

Fig. 6. Control effect comparison curve

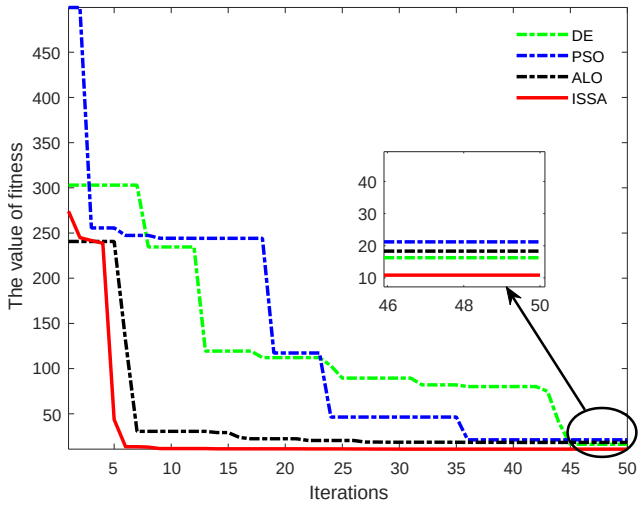

Fig. 7. Convergence curves for each algorithm

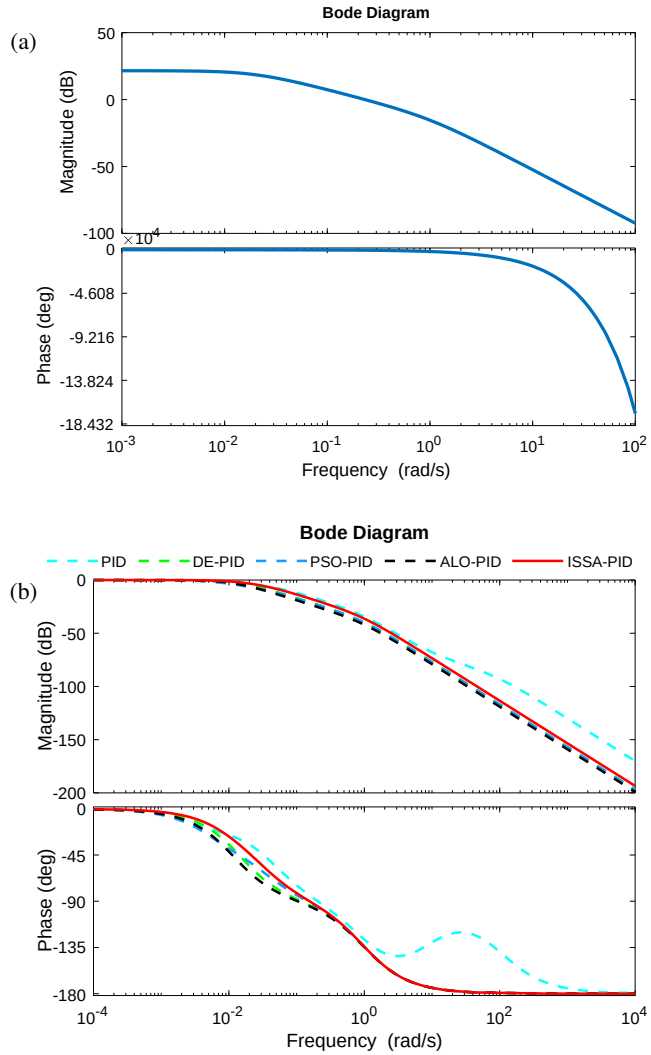

Fig. 8. Comparison of Bode plots between different controllers (where (a) is the Bode plot without any controller, and (b) is the Bode curve of each PID controller)

The data in Fig. 6 is analyzed to obtain the performance metrics for each algorithmic curve, as shown in Table 4. ISSA-PID, compared with PID, DE-PID, PSO-PID and ALO-PID, in terms of maximum overshoot σ, produces 0.0107% overshooting, but is 3.3453%, 1.8366% and 0.5558% less than PID, DE-PID and ALO-PID; in terms of peak time t_p, it is slower than PID and DE-PID, but is reduced by 970 s and 95 s in comparison with PSO-PID and ALO-PID; in terms of rise time t_r, it is slower than PID, but is still 35 s, 150 s and 80 s less than DE-PID, PSO-PID and ALO-PID; regarding stable time t_s, ISSA takes the least time, with a reduction of 356.3 s, 30 s, 225 s and 110 s as compared to PID, DE-PID, PSO-PID and ALO-PID. Also, as seen from the convergence graph in Fig. 7, ISSA has the fastest convergence rate. Therefore, ISSA-PID is superior in overall performance.

The comparative Bode plots of the chilled water control system with different controllers are shown in Fig. 8. The comparative frequency response performance analysis results such as gain margin (in decibel), phase margin (in degrees) and bandwidth (in Hertz) are presented in Table 5, respectively. It is observed from the table that the bandwidth of ISSA-PID is larger than that of other controllers. This shows that ISSA-PID also performs better in terms of stability regarding the frequency response criterion.

Table 5
Comparative frequency response performance analysis results

Controller type	Gain margin (dB)	Phase margin (deg.)	Bandwidth (Hz)
PID	∞	180	(0, 0.0362]
DE-PID	∞	180	(0, 0.0484]
PSO-PID	∞	180	(0, 0.0279]
ALO-PID	∞	180	(0, 0.0363]
ISSA-PID	∞	180	(0, 0.0607]

5.1.1. Lifting load test

After the system response curve is stabilized, the set value of the step response is increased from 1 to 1.4 at 1250 s, and the simulation time is 2500 s. The response curve is shown in Fig. 9.

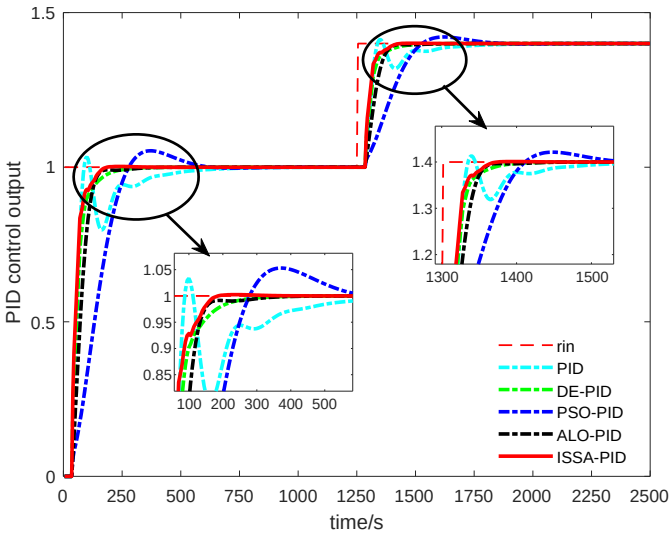

Fig. 9. Lifting load response curve

The maximum overshoot σ, peak time t_p, rise time t_r and stable time t_s (minimum time to stabilize within $\pm 2\%$ error) after increasing the load are obtained in the analysis of Fig. 9. The data are shown in Table 6.

Table 6
Performance index

Algorithm	$\sigma(\%)$	t_p(s)	t_r (s)	t_s(s)
PID	1.335	100	62	233.5
DE-PID	0	520	65	142.5
PSO-PID	2.12	365	165	241
ALO-PID	0	540	85	131.5
ISSA-PID	0.1	230	60	121

Table 6 is analyzed to compare the performance metrics of each controller after 1250 s of increased load. Under the condition that each PID controller parameter is kept constant, ISSA-PID produces 0.1% overshoot; but in terms of peak time, it is reduced by 290 s, 80 s, 310 s as compared with DE-PID, PSO-PID, ALO-PID, respectively. In terms of rise time, it is reduced by 2 s, 5 s, 95 s and 85 s as compared with PID, DE-PID, PSO-PID and ALO-PID, respectively; in terms of stable time, ISSA-PID is reduced by 112.5 s, 21.5 s, 321 s and 10.5 s as compared with PID, DE-PID, PSO-PID and ALO-PID, respectively. The transient response speed of ISSA-PID is superior to the rest of the algorithms. The above show the superiority of ISSA-PID in control accuracy and response speed in lifting loads.

5.1.2. Perturbation test

After the system is stabilized, a 25 s perturbation is applied at 1250 s to test the immunity of the algorithm. And the simulation time is 2500 s. To minimize its effect on the system performance, the designed controller must suppress it quickly. The system response curve is shown in Fig. 10.

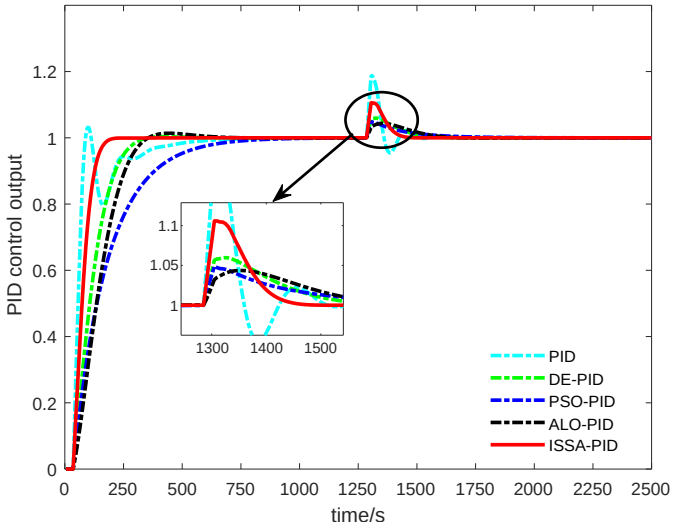

Fig. 10. Response curve of the applied disturbance

A 1.4-step signal is applied at 1250 s and supplied for 25 s. Under the condition that the parameters of each PID controller remain constant, the time needed for various controllers to recover their outputs to within a 2% error after being disturbed by the step signal is compared, as shown in Table 7.

Table 7
Recovery time

Algorithm	Recovery time (s)
PID	215
DE-PID	201
PSO-PID	183.5
ALO-PID	235
ISSA-PID	147.5

ISSA-PID keeps the output of PID within the 2% error in the shortest time, 67.5 s faster than PID, 53 s faster than DE-PID, 36 s faster than PSO-PID, and 87.5 s faster than ALO-PID. It is further verified that the ISSA-PID controller is characterized by more anti-interference than other controllers.

5.2. Battery charging systems

The battery charging process has the characteristics of nonlinearity and hysteresis, and it is difficult for the conventional PID parameter tuning method to give the appropriate parameters and thus, the charging efficiency of the battery is affected inevitably. The equivalent model of its charging system can be expressed in Fig. 11.

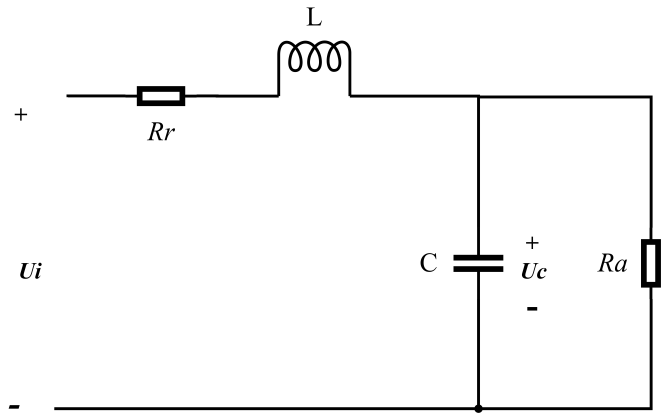

where Rr is the internal resistance of the rectifier module; Ra is the internal resistance of the battery; Ui is the ideal voltage of the rectifier device and Uc is the charging voltage of the battery

Fig. 11. Battery charging system equivalent circuit

In thyristor rectifier modules, the dynamically triggered rectifier portion is a purely delayed amplification section, which is mainly due to the uncontrolled timing of the rectifier module. In a certain range of work, using linear transformation for the rectifier output UI and control voltage Uc, UI lags behind by $KS = \Delta UI/\Delta Uc$ namely [28]:

$$\frac{UI(s)}{Uc(s)} = K_s e^{-T_s s}. \tag{14}$$

Thus, equation (15) is the transfer function of the battery charging system.

$$G(s) = \frac{R_a}{R_r + R_a + Ls + R_r R_a Cs} K_s e^{-Ts}, \tag{15}$$

Bringing $L = 50$ mH, $C = 5$ F, $R_r \approx 0.8$, $R_a \approx 0.2\ \Omega$, $K_s = 5$, $T_s = 0.067$ s, $T_1 = 0.028$ s, $T = T_1 + T_s = 0.095$ s into equation (15), the final controlled transfer function [28] is given by equation (16).

$$G(s) = \frac{e^{-0.095s}}{0.8s + 1}. \tag{16}$$

The validation is done against PID, DE-PID, PSO-PID and ALO-PID with time as a variable and unit step signal as input. The sampling period of each algorithm is 0.095 s, and the simulation time is 6 s. The PID controller parameters of the battery charging system are calibrated by the Z–N tuning method, and the conventional PID parameters are $K_p = 1.9$, $K_i = 2.2$ and $K_d = 0.25$ after several trials. Then, the parameters of the five PID controllers are shown in Table 8, the control effect comparison graph is shown in Fig. 12, the convergence curve is shown in Fig. 13, the Bode curve is shown in Fig. 14, and the performance index of each algorithm is shown in Table 9.

The data in Fig. 12 are analyzed to obtain the performance metrics of each algorithmic curve, as shown in Table 9. ISSA-PID showed a reduction of 1.591 s, 2.539 s, 3.336 s and 1.269 s in peak time t_p as compared to PID, DE-PID, PSO-PID and ALO-PID, respectively; in terms of rise time t_r, ISSA was reduced by 0.661 s, 0.13 s, 0.224 s and 0.111 s as compared to PID, DE-PID, PSO-PID and ALO-PID, respectively; regarding stable time t_s, ISSA-PID decreased by 1.305 s, 0.23 s, 0.306 s and 0.43 s as compared to PID, DE-PID, PSO-PID and ALO-PID, respectively. Also, it can be seen from Fig. 13 that ISSA has the fastest convergence rate.

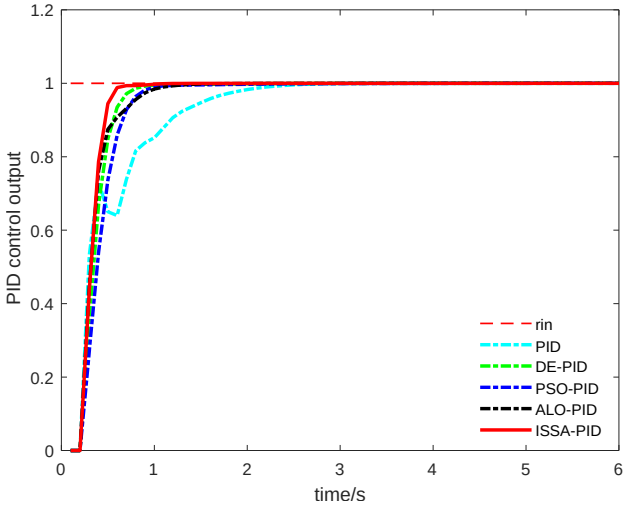

Fig. 12. Control effect comparison curve

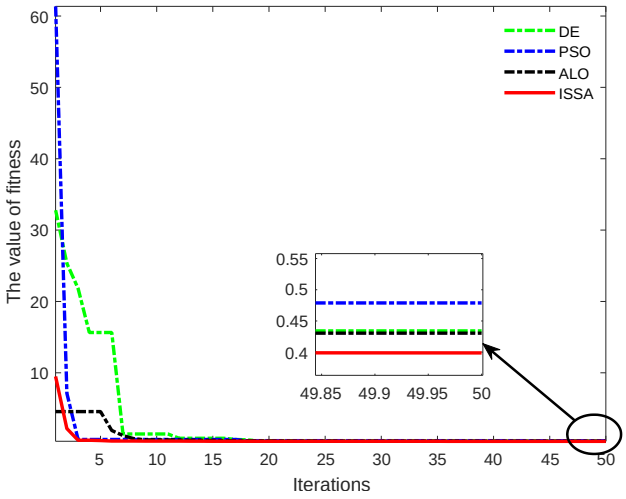

Fig. 13. Convergence curves for each algorithm

Table 8
PID parameters

Algorithm	K_p	K_i	K_d	$J(t)$
PID	1.9	2.2	0.25	—
DE-PID	2.5123	3.2202	0.037682	0.43405
PSO-PID	2.1539	2.7742	0	0.47887
ALO-PID	2.6242	3.2949	0.10058	0.4304
ISSA-PID	2.9129	3.7281	0.076291	0.39879

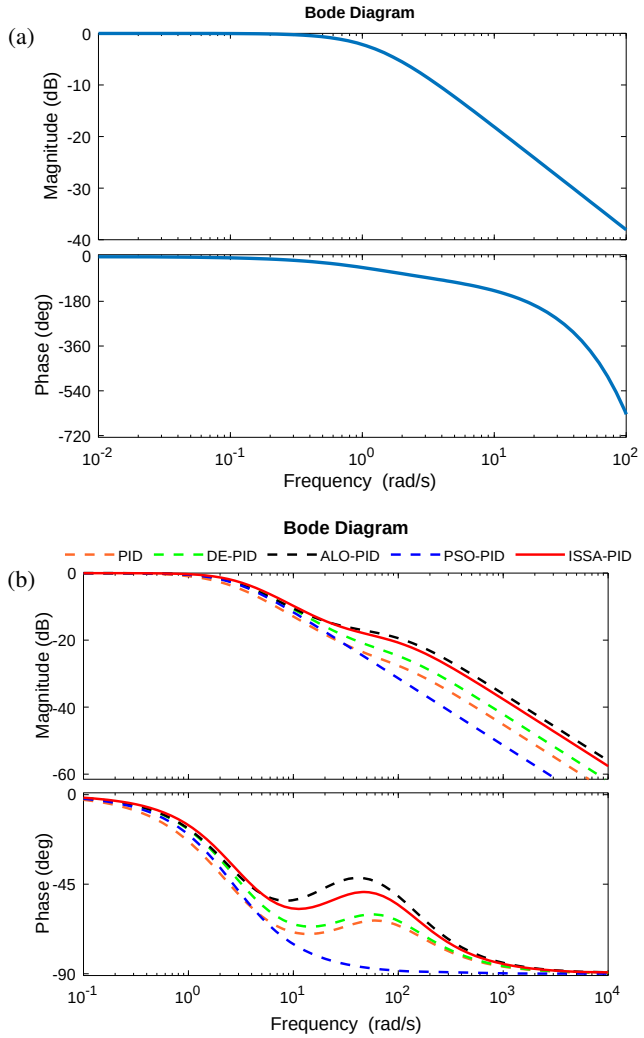

Fig. 14. Comparative Bode plots for different controllers: (a) is the Bode plot without any controller, and (b) is the Bode curve of each PID controller

Table 9
Performance index

Algorithm	$\sigma(\%)$	t_p(s)	t_r (s)	t_s(s)
PID	0.09	3.747	1.182	1.92
DE-PID	0	4.695	0.651	0.845
PSO-PID	0	5.492	0.745	0.921
ALO-PID	0	3.425	0.632	1.045
ISSA-PID	0	2.156	0.521	0.615

The comparative Bode plots of the battery charging system with different controllers are shown in Fig. 14, respectively. The comparative frequency response performance analysis results such as gain margin (in decibel), phase margin (in degrees) and bandwidth (in Hertz) are presented in Table 10, correspondingly. It can be found from the table that the bandwidth of ISSA-PID is larger than that of other controllers. This indicates that

Table 10
Comparative frequency response performance analysis results

Controller type	Gain margin (dB)	Phase margin (deg.)	Bandwidth (Hz)
PID	∞	180	(0, 6.37]
DE-PID	∞	180	(0, 9.52]
PSO-PID	∞	180	(0, 8.50]
ALO-PID	∞	180	(0, 8.83]
ISSA-PID	∞	180	(0, 10.5]

the stability of ISSA-PID is also better in terms of the frequency response standard.

5.2.1. Lifting load test

After the system response curve is stabilized, the set value of the step response is increased from 1 to 1.4 at 5 s, and the simulation time is 10 s. The response curve is shown in Fig. 15.

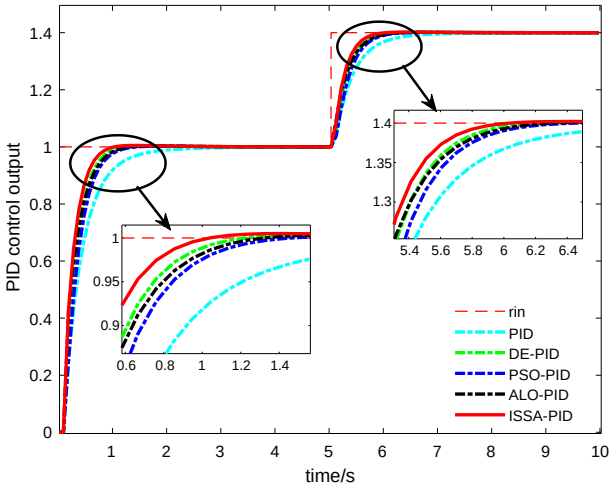

Fig. 15. Lifting load response curve

The maximum overshoot σ, peak time t_p, rise time t_r and stable time t_s after 5 s of increased load are obtained in Fig. 15, and the data are listed in Table 11.

Under the condition that the parameters of each PID controller remain constant, the performance indices of each con-

Table 11
Performance index

Algorithm	σ (%)	t_p (s)	t_r (s)	t_s (s)
PID	0	3.265	0.48	1.01
DE-PID	1.45	1.55	0.37	0.69
PSO-PID	0.88	1.84	0.40	0.77
ALO-PID	1.52	1.745	0.32	0.72
ISSA-PID	1.89	1.27	0.30	0.59

troller are compared after the load increases to 5 s. The maximum overshoot is maintained within 2% for each algorithm; in terms of peak time, ISSA-PID was reduced by 1.995 s, 0.28 s, 0.57 s and 0.475 s as compared to PID, DE-PID, PSO-PID and ALO-PID, respectively; in terms of rise time, it was reduced by 0.179 s, 0.069 s, 0.101 s and 0.019 s as compared to PID, DE-PID, PSO-PID and ALO-PID, respectively; regarding stable time, ISSA-PID is shorter than PID, DE-PID, PSO-PID and ALO-PID by 0.4225 s, 0.1 s, 0.175 s and 0.13 s, also respectively. And the transient response speed of ISSA-PID is also superior to the rest of the algorithms. The above show the superiority of ISSA-PID in control accuracy and response speed in rising loads.

5.2.2. Perturbation test

After the system is stabilized, a perturbation of 0.2 s is applied at 1250 s to test the immunity of the algorithm. The simulation time is 2500 s. The system response curve is shown in Fig. 16.

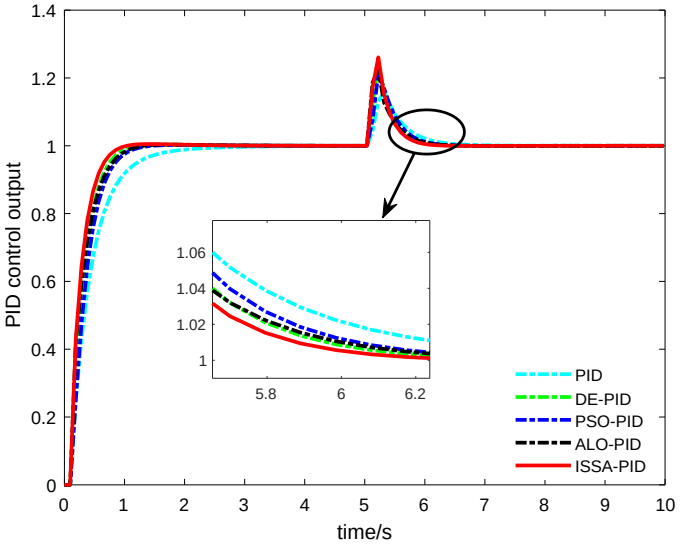

Fig. 16. Response curve of the applied disturbance

When analyzing Fig. 16, a 1.4-step signal is applied at 5 s and lasts for 0.2 s, with the parameters of each PID controller held constant. A comparison of the time needed for various controllers to recover their outputs to within a 2% error after being disturbed by the step signal is shown in Table 12.

Table 12
Recovery time

Algorithm	Recovery time (s)
PID	0.985
DE-PID	0.795
PSO-PID	0.824
ALO-PID	0.813
ISSA-PID	0.712

ISSA-PID keeps the output of the PID controller within the 2% error in the shortest time, of which time is 0.273 s, 0.083 s, 0.112 s and 0.101 s faster than that of PID, DE-PID, PSO-PID and ALO-PID, respectively. This verifies that the ISSA-PID controller is characterized by more anti-interference than other controllers.

6. CONCLUSIONS

This paper proposes an ISSA based on SSA. The ISSA is verified to have better convergence speed and accuracy by comparison with PSO, GWO, WOA and SSA through nine benchmark test functions. And to test the optimization performance of PID controller parameters by ISSA, the chilled water control system and the battery charging system are used as examples to compare with PID, DE-PID, PSO-PID and ALO-PID for the tests of lifting the load and applying perturbation. The results show that ISSA-PID improves the convergence speed, accuracy, anti-interference ability and robustness as compared to the other four PID controllers.

ACKNOWLEDGEMENTS

The authors are grateful to the referees who have contributed to enhance the technical content of this paper. This Project is supported by the key research and development program for Natural Science Foundation of Liaoning Province (No. 2023JH2/101300218) and the cooperative program for Intelligent Industry Foundation of Anshan Iron and Steel Corporation (No. 2020-KD-1001).

REFERENCES

[1] D. Wei, Z. Wang, L. Si, and C. Tan, "Preaching-inspired swarm intelligence algorithm and its applications," *Knowledge-Based Syst.*, vol. 211, p. 106552, 2021, doi: 10.1016/j.knosys.2020.106552.

[2] S.B. Joseph, E.G. Dada, A. Abidemi, D.O. Oyewola, and B.M. Khammas, "Metaheuristic algorithms for PID controller parameters tuning: review, approaches and open problems," *Heliyon*, vol. 8, no. 5, p. e09399, 2022, doi: 10.1016/j.heliyon.2022.e09399.

[3] A. Najm and I. K. Ibraheem, "Nonlinear PID controller design for a 6-DOF UAV quadrotor system," *Eng. Sci. Technol.*, vol. 22, no. 4, pp. 1087–1097, 2019, doi: 10.1016/j.jestch.2019.02.005.

[4] P.N. Pugazhenthi, S. Selvaperumal, and K. Vijayakumar, "Nonlinear PID controller parameter optimization using modified hybrid artificial bee colony algorithm for continuous stirred tank reactor," *Bull. Pol. Acad. Sci. Tech. Sci.*, vol. 69, no. 3, p. e137348, 2021, doi: 10.24425/bpasts.2021.137348.

[5] V. Vishnoi, S. Tiwari, and R. Singla, "Performance Analysis of Moth Flame Optimization-Based Split-Range PID Controller," *Mapan*, vol. 36, no. 1, pp. 67–79, 2020, doi: 10.1007/s12647-020-00379-0.

[6] A. Manjula, L. Kalaivani, M. Gengaraj, R.V. Maheswari, S. Vimal, and S. Kadry, "Performance enhancement of SRM using smart bacterial foraging optimization algorithm based speed and current PID controllers," *Comput. Electr. Eng.*, vol. 95, p. 107398, 2021, doi: 10.1016/j.compeleceng.2021.107398.

[7] L. Dai, H. Lu, D. Hua, X. Liu, L. Wang, and Q. Li, "Research on Control Strategy of a Magnetorheological Fluid Brake Based on an Enhanced Gray Wolf Optimization Algorithm," *Appl. Sci.*, vol. 12, no. 24, p. 12617, 2022, doi: 10.3390/app122412617.

[8] J.-Y. Cao and B.-G. Cao, "Design of Fractional Order Controllers Based on Particle Swarm Optimization," *2006 1st IEEE conference on industrial electronics and applications*. IEEE, 2006.

[9] N. Soundirarrajan and K. Srinivasan, "Performance Evaluation of Ant Lion Optimizer–Based PID Controller for Speed Control of PMSM," *J. Test. Eval.*, vol. 49, no. 2, pp. 1104–1118, 2019, doi: 10.1520/JTE20180892.

[10] D. Potnuru, K. Alice Mary, and Ch. Sai Babu, "Experimental implementation of Flower Pollination Algorithm for speed controller of a BLDC motor," *Ain Shams Eng. J.*, vol. 10, no. 2, pp. 287–295, 2019, doi: 10.1016/j.asej.2018.07.005.

[11] K. Cao, Z. Li, Y. Gu, L. Zhang, and L. Chen, "The control design of transverse interconnected electronic control air suspension based on seeker optimization algorithm," *Proc. Inst. Mech. Eng. Part D-J. Automob. Eng.*, vol. 235, no. 8, pp. 2200–2211, 2021, doi: 10.1177/0954407020984667.

[12] H. Naga Sai Kalyan *et al.*, "Seagull Optimization Algorithm–Based Fractional-Order Fuzzy Controller for LFC of Multi-Area Diverse Source System With Realistic Constraints," *Front. Energy Res.*, vol. 10, 2022, doi: 10.3389/fenrg.2022.921426.

[13] Q. Jin, L. Qi, B. Jiang, and Q. Wang, "Novel improved cuckoo search for PID controller design," *Trans. Inst. Meas. Control*, vol. 37, no. 6, pp. 721–731, 2014, doi: 10.1177/0142331214544211.

[14] J. Xue and B. Shen, "A novel swarm intelligence optimization approach: sparrow search algorithm," *Syst. Sci. Control Eng.*, vol. 8, no. 1, pp. 22–34, 2020, doi: 10.1080/21642583.2019.1708830.

[15] D. Wu, and C. Yuan, "Threshold image segmentation based on improved sparrow search algorithm," *Multimed. Tools Appl.*, vol. 81, no. 23, pp. 33513–33546, 2022, doi: 10.1007/s11042-022-13073-x.

[16] Z. Zhang, R. He, and K. Yang, "A bioinspired path planning approach for mobile robots based on improved sparrow search algorithm," *Adv. Manuf.*, vol. 10, no. 1, pp. 114–130, 2021, doi: 10.1007/s40436-021-00366-x.

[17] G. Liu, C. Shu, Z. Liang, B. Peng, and L. Cheng, "A Modified Sparrow Search Algorithm with Application in 3d Route Planning for UAV," *Sensors (Basel)*, vol. 21, no. 4, p. 1224, 2021, doi: 10.3390/s21041224.

[18] X. Zhou, J. Wang, H. Zhang, and Q. Duan, "Application of a hybrid improved sparrow search algorithm for the prediction and control of dissolved oxygen in the aquaculture industry," *Appl. Intell.*, vol. 53, no. 7, pp. 8482–8502, 2023, doi: 10.1007/s10489-022-03870-0.

[19] J. Hou, X. Wang, Y. Su, Y. Yang, and T. Gao, "Parameter Identification of Lithium Battery Model Based on Chaotic Quantum Sparrow Search Algorithm," *Appl. Intell.*, vol. 12, no. 14, 2022, doi: 10.3390/app12147332.

[20] X. Li, J. Gu, X. Sun, J. Li, and S. Tang, "Parameter identification of robot manipulators with unknown payloads using an improved chaotic sparrow search algorithm," *Appl. Intell.*, vol. 52, no. 9, pp. 10341–10351, 2022, doi: 10.1007/s10489-021-02972-5.

[21] Ch. Ouyang, F. Tang, D. Zhu, Y. Qiu, and Y. Liu, "Application of Improved Sparrow Search Algorithm in Concrete," *J. Phys.-Conf. Ser.*, vol. 2082, p. 012014, 2021, doi: 10.1088/1742-6596/2082/1/012014.

[22] X. Lv, X. Mu, J. Zhang, and Z. Wang, "Chaos Sparrow Search Optimization Algorithm," *J. Beijing Univ. Aeronaut. Astronaut.*, vol. 47, no. 08, pp. 1712–1720, 2021, doi: 10.13700/j.bh.1001-5965.2020.0298.

[23] Y. Fan, J. Shao, and G. Sun, "Optimized PID Controller Based on Beetle Antennae Search Algorithm for Electro-Hydraulic Position Servo Control System," *Sensors*, vol. 19, no. 12, p. 2727, 2019, doi: 10.3390/s19122727.

[24] Guo, Z. Zhuang, J.-S. Pan, and S.-C. Chu, "Optimal Design and Simulation for PID Controller Using Fractional-Order Fish Migration Optimization Algorithm," *IEEE Access*, vol. 9, pp. 8808–8819, 2021, doi: 10.1109/access.2021.3049421.

[25] Ashmi M, Anila M, Sivanandan K S, Jayaraj S, "Comparison of Z–N and PSO based tuning methods in the control strategy of prosthetic limbs application," *Journal of Theoretical and Applied Mechanics*, vol.58, no. 4, pp. 841–851, 2020, doi: 10.15632/jtam-pl/125505.

[26] M. Ouyang, Y. Wang Y, Wu F, and Lin Y, "Continuous Reactor Temperature Control with Optimized PID Parameters Based on Improved Sparrow Algorithm," *Processes*, vol.11, no. 5, pp. 1302, 2023, doi: 10.3390/pr11051302.

[27] Q. Zhu, M. Zhuang, H. Liu, and Y. Zhu, "Optimal Control of Chilled Water System Based on Improved Sparrow Search Algorithm," *Buildings*, vol. 12, no. 3, 2022, doi: 10.3390/buildings12030269.

[28] T. Wu, C. Zhou, Z. Yan, H. Peng, and L. Wu, "Application of PID optimization control strategy based on particle swarm optimization (PSO) for battery charging system," *International Journal of Low-Carbon Technologies*, vol. 15, no. 4, pp. 528–535, 2020, doi: 10.1093/ijlct/ctaa020.